TU Delft

Delft University of Technology

Document Version
Final published version

Licence
Dutch Copyright Act (Article 25fa)

Citation (APA)
Riccardi, A., Laurenti, L., & De Schutter, B. (2025). A benchmark for multi-agent control of energy systems: The European economic area hybrid electricity network benchmark *. In *Proceedings of the 23rd European Control Conference (ECC 2025)* (pp. 2575-2582). IEEE. https://doi.org/10.23919/ECC65951.2025.11187247

Important note
To cite this publication, please use the final published version (if applicable).
Please check the document version above.

Copyright
In case the licence states “Dutch Copyright Act (Article 25fa)”, this publication was made available Green Open Access via the TU Delft Institutional Repository pursuant to Dutch Copyright Act (Article 25fa, the Taverne amendment). This provision does not affect copyright ownership.
Unless copyright is transferred by contract or statute, it remains with the copyright holder.

Sharing and reuse
Other than for strictly personal use, it is not permitted to download, forward or distribute the text or part of it, without the consent of the author(s) and/or copyright holder(s), unless the work is under an open content license such as Creative Commons.

Takedown policy
Please contact us and provide details if you believe this document breaches copyrights.
We will remove access to the work immediately and investigate your claim.

This work is downloaded from Delft University of Technology.

2025 23rd European Control Conference (ECC)
June 24-27, 2025. Thessaloniki, Greece

A benchmark for multi-agent control of energy systems: The European economic area hybrid electricity network benchmark*

Alessandro Riccardi[1], Luca Laurenti[1], and Bart De Schutter[1]

Abstract— **In this paper, we present a control-oriented benchmark of a network of dynamical systems representing an abstraction of the European Economic Area (EEA) electricity network. In the network each node represents a country of the EEA as an equivalent electrical area with specific generation and load features. The benchmark has been developed to provide the research community with a tool to assess non-centralized control strategies over a standardized case study. The Load Frequency Control (LFC) problem in the presence of renewable energy sources is considered, where the objective is to maintain a nominal operating frequency of the electricity network despite the presence of variations in the load request, and renewable energy production. A hybrid implementation of Energy Storage Systems (ESSs) with different operating modes is considered in the network to support energy generation. We test the features of the system through control simulations with centralized Model Predictive Control (MPC), and a Distributed MPC (DMPC) based on the Alternating Direction Method of Multipliers (ADMM). The benchmark is provided together with a long-term access repository containing both the data, and the scripts to access and process the data.**

I. INTRODUCTION

The development of non-centralized control strategies is an active field of research. This attention is motivated by the challenges that modern systems are posing, both in terms of complexity and scale [1, 2]. Often, such systems are composed by multiple agents [3], where an agent is defined as an individual entity of a network that can exert some form of control or decision-making capability. Several approaches have been sought in the literature to address the problem of controlling multi-agent systems, such as decentralized control [4], non-centralized Model Predictive Control (MPC) [5], coalitional control [6], and multi-agent reinforcement learning [7]. In real world networks, the challenges are exacerbated by the fact that systems often exhibit hybrid dynamics, which may include the presence of logic-driven behaviors, integration of discrete-time and continuous-time systems, and configuration-dependent dynamics. Such characteristics can be represented by hybrid systems [8], which represent a direct extension of linear systems into the nonlinear domain [9], and allow for the inclusion of logical statements [10, 11]. Control architectures applied to hybrid systems have been developed, e.g. for electricity networks [12, 13, 14], transportation networks [15], water networks [16], and other fields [17].

However, despite the great interest for the field and the volume of research, when referring to multi-agent systems, there is a lack of standardized benchmarks to test these methods. Consequently, it is often difficult to compare the different approaches directly, because they are validated through different case studies or even case studies in different fields. To address this necessity of coherence in the comparison of different non-centralized control approaches, in this paper we develop a benchmark based on energy networks, which are among the most relevant application domains for control engineering. The benchmark is open-access and made available on the long-term access repository [18] containing the Python scripts to perform the operations reported, the prepared dataset, and further technical documentation.

In this benchmark, we combine topological information, electricity data, and the mathematical modeling of an electrical area to obtain a network of hybrid dynamical systems suited for the direct implementation of a control strategy. The electrical areas are selected to coincide with the countries of the European Economic Area (EEA), and exploit official topological and electrical data. We will refer to the benchmark as the European Economic Area Hybrid Electricity Network Benchmark (EEA-HENB), which is an extension of the benchmark we developed in [19, 20] for linear systems, and used to test partitioning strategies for DMPC in [21, 22]. Specifically, we extend this previous work by incorporating official topological data for accurate computation of the network topology, implementing different charging modes for the ESS, and providing a ready-to-use distributed implementation of MPC. Throughout this paper, we illustrate how to use a combination of data and conventional modeling techniques to obtain a hybrid model.

The motivation for developing this benchmark for multi-agent energy networks can be sought in the current challenges and opportunities that such systems provide, such as the expansion in the adoption of distributed energy resources, as well as the ever-increasing energy demand, and the ease of accessibility to high-speed communication infrastructures [23]. In particular, one of the most studied problems for energy networks that is also directly impacted by these recent developments is the Load Frequency Control (LFC) problem [24, 25]. The LFC problem consists of maintaining the deviation of the frequency of an energy network w.r.t. the nominal operating frequency within safe intervals, despite the presence of variations in the load demand, and in the power produced by renewable energy sources. Moreover, the use of

*This project has received funding from the European Research Council (ERC) under the European Union's Horizon 2020 research and innovation program (Grant agreement No. 101018826) – Project CLariNet.

[1]A. Riccardi, L. Laurenti, and B. De Schutter are with the Delft Center for Systems and Control (DCSC), Delft University of Technology, Delft, The Netherlands.

Corresponding author: A. Riccardi, a.riccardi@tudelft.nl

Authorized licensed use limited to: TU Delft Library. Downloaded on April 21,2026 at 11:19:51 UTC from IEEE Xplore. Restrictions apply.

hybrid dynamical formulations in the LFC problem allows to extend the types of phenomena that can be represented, which include hybrid Energy Storage System (ESS) [26, 27] with varying energy exchange rates. Currently, no benchmark is used consistently as a standard to test control strategies for hybrid formulations of the LFC problem.

The paper is structured as follows: the topological and electricity data used in the benchmark are reported in Section III; the mathematical models used in the benchmark are presented in detail in Section IV; and the comparison of centralized and distributed predictive control strategies is performed in Section V. We conclude highlighting the future directions for its further development in Section VI.

II. NOTATION

In this benchmark, we model each country of the EEA as an equivalent electrical area aggregating all the dispatchable power sources, loads, and renewable sources. The area i will be denoted by $\mathcal{A}_i$. Each $\mathcal{A}_i$ will be represented by the combination of a set of data presented in Section III and an equivalent electrical area model described by the system of hybrid difference equations presented in Section IV.

The topological information about the electricity network is represented using a graph $\mathcal{G} = (\mathcal{V}, \mathcal{E})$ associated with the network of agents. Here, the set of nodes is $\mathcal{V} = \{\mathcal{A}_1, \dots, \mathcal{A}_N\}$, where N is the number of electrical areas in the network, and a set of edges is $\mathcal{E} = \{(i,j) \,|\, i,j \in \mathcal{V}\}$, where an edge (i,j) exists if and only if a connection between $\mathcal{A}_i$ and $\mathcal{A}_j$ exists in the network topology. For a given node $i \in \mathcal{V}$, the set of all nodes connected to i is called the neighborhood of i, and denoted by $\mathcal{N}_i = \{j \in \mathcal{V} \mid (i,j) \in \mathcal{E}\}$.

III. TOPOLOGICAL AND ELECTRICAL DATA

A. Network Topology

We determine the topology of the network from the geographical information provided by the Geographic Information System of the COmmission (GISCO) of the statistical office of the European Union (Eurostat). The dataset is available at [28], and it is provided by GISCO as a nomenclature of territorial units for statistics, also called NUTS. These data are thus processed to establish the locations of the electrical areas $\mathcal{A}_i$, which we assume to coincide with the geographical centroid of the respective country, as further explained in [18]. The resulting coordinates are listed in Table I. To determine the connections between the equivalent electrical areas we use the ENTSO-E transmission system map available at [29], thus establishing the electrical topology of the network. Then, we compute the distances between the equivalent electrical areas using the Euclidean distance, thus determining the lengths of the tie-lines. The resulting weighted adjacency matrix W_{adj} is reported in Table II, where each entry w_{ij} corresponds to the distance between the electrical areas i and j expressed in 10^3 [km]. We denote the binary version of W_{adj} with A_{adj}, and its entries are equal to one for each nonzero corresponding entry of W_{adj}, and zero otherwise. Combining geographical and electrical information, we obtain the graphical representation of the electrical topology of the EEE-HENB represented in Fig. 1.

TABLE I: Coordinates of the centroids in the system ETRS89 LAEA [$\times 10^6$], and installed capacity in [GW].

ID	Area	ISO	X	Y	Capacity [GW]
01	Austria	AT	4.63	2.73	7.471
02	Belgium	BE	3.94	3.07	13.879
03	Bulgaria	BG	5.56	2.31	9.706
04	Croatia	HR	4.83	2.46	2.609
05	Czech Republic	CZ	4.71	2.97	15.273
06	Denmark	DK	4.33	3.65	7.660
07	Estonia	EE	5.22	4.05	1.685
08	Finland	FI	5.10	4.66	10.935
09	France	FR	2.91	2.36	90.510
10	Germany	DE	4.35	3.10	87.408
11	Greece	GR	5.45	1.87	9.723
12	Hungary	HU	5.03	2.72	7.608
13	Ireland	IE	3.12	3.49	7.400
14	Italy	IT	4.50	2.18	59.551
15	Latvia	LV	5.23	3.85	1.326
16	Lithuania	LT	5.20	3.67	1.659
17	Netherlands	NL	4.02	3.25	23.595
18	Norway	NO	4.45	4.81	27.353
19	Poland	PL	4.96	3.26	33.752
20	Portugal	PT	2.74	2.03	8.056
21	Romania	RO	5.48	2.64	9.664
22	Slovakia	SK	5.02	2.89	4.737
23	Slovenia	SI	4.69	2.57	2.329
24	Spain	ES	3.16	2.01	62.362
25	Sweden	SE	4.65	4.38	31.600
26	Switzerland	CH	4.19	2.63	8.558

B. Electricity Data, Capacities, and Bounds

Electricity data are acquired from the European Network of Transmission Systems Operators (ENTSO)-E transparency platform [30]. The platform provides data about the power generation and the load request. Specifically, for each country in the EEA the following data is available: i) day-ahead load request forecast; ii) measured load request; iii) day-ahead renewable generation forecast; iv) measured renewable generation. We acquire data for one day of operation of the network, which is January 1, 2022, and the resulting power profiles for each area can be found in [19]. We pre-process this data as described in [18] so that we can perform a simulation of the system with a sampling time $\tau = 0.25$ [s]. The resulting incremental power variations are in [19].

We obtain different electricity profiles for each area, which correspond to different production capacities. To account for this aspect, we establish bounds for the maximum dispatchable capacity of each country, considering data about the installed capacities per production type available at [30]. The resulting total capacities are given in the last column of Table I. The minimal capacity is assumed to be 0 [GW], i.e. direct energy dissipation is not allowed.

Authorized licensed use limited to: TU Delft Library. Downloaded on April 21,2026 at 11:19:51 UTC from IEEE Xplore. Restrictions apply.

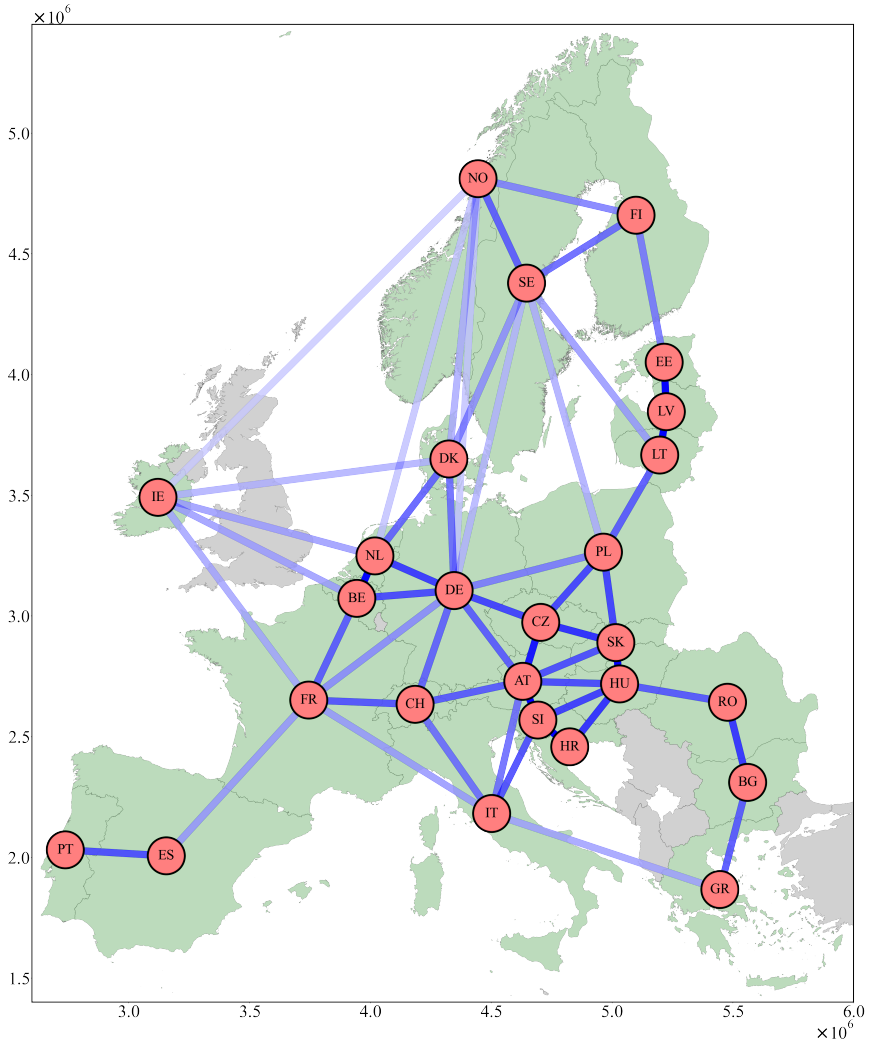

Fig. 1: Electrical topology of the EEA equivalent electricity network. Each node corresponds to a country, and it is labeled with the respective ISO code. Coordinates are expressed in the system ETRS89 LAEA. The edges of the graph represent the tie-lines connecting the equivalent electrical areas, and their transparency is the strenght of the interaction.

TABLE II: Lengths of the tie-lines expressed in 10^3 [km].

ISO	AT	BE	BG	HR	CZ	DK	EE	FI	FR	DE	GR	HU	IE	IT	LV	LT	NL	NO	PL	PT	RO	SK	SI	ES	SE	CH
AT	0	0	0	0	0.26	0	0	0	0	0.47	0	0.4	0	0.56	0	0	0	0	0	0	0	0.42	0.17	0	0	0.46
BE	0	0	0	0	0	0	0	0	0.47	0.4	0	0	0.92	0	0	0	0.19	0	0	0	0	0	0	0	0	0
BG	0	0	0	0	0	0	0	0	0	0	0.46	0	0	0	0	0	0	0	0	0	0.34	0	0	0	0	0
HR	0	0	0	0	0	0	0	0	0	0	0	0.33	0	0	0	0	0	0	0	0	0	0	0.17	0	0	0
CZ	0.26	0	0	0	0	0	0	0	0	0.38	0	0	0	0	0	0	0	0	0.39	0	0	0.32	0	0	0	0
DK	0	0	0	0	0	0	0	0	0	0.55	0	0	1.21	0	0	0	0.5	1.17	0	0	0	0	0	0	0.8	0
EE	0	0	0	0	0	0	0	0.62	0	0	0	0	0	0	0.21	0	0	0	0	0	0	0	0	0	0	0
FI	0	0	0	0	0	0	0.62	0	0	0	0	0	0	0	0	0	0	0.67	0	0	0	0	0	0	0.53	0
FR	0	0.47	0	0	0	0	0	0	0	0.75	0	0	1.05	0.89	0	0	0	0	0	0	0	0	0	0.87	0	0.44
DE	0.47	0.4	0	0	0.38	0.55	0	0	0.75	0	0	0	0	0	0	0	0.36	1.71	0.64	0	0	0	0	0	1.31	0.5
GR	0	0	0.46	0	0	0	0	0	0	0	0	0	0	1	0	0	0	0	0	0	0	0	0	0	0	0
HU	0.4	0	0	0.33	0	0	0	0	0	0	0	0	0	0	0	0	0	0	0	0	0.45	0.17	0.37	0	0	0
IE	0	0.92	0	0	0	1.21	0	0	1.05	0	0	0	0	0	0	0	0.93	1.87	0	0	0	0	0	0	0	0
IT	0.56	0	0	0	0	0	0	0	0.89	0	1	0	0	0	0	0	0	0	0	0	0	0	0.43	0	0	0.55
LV	0	0	0	0	0	0	0.21	0	0	0	0	0	0	0	0	0.18	0	0	0	0	0	0	0	0	0	0
LT	0	0	0	0	0	0	0	0	0	0	0	0	0	0	0.18	0	0	0	0.46	0	0	0	0	0	0.9	0
NL	0	0.19	0	0	0	0.5	0	0	0	0.36	0	0	0.93	0	0	0	0	1.62	0	0	0	0	0	0	0	0
NO	0	0	0	0	0	1.17	0	0.67	0	1.71	0	0	1.87	0	0	0	1.62	0	0	0	0	0	0	0	0.48	0
PL	0	0	0	0	0.39	0	0	0	0	0.64	0	0	0	0	0	0.46	0	0	0	0	0	0.38	0	0	1.16	0
PT	0	0	0	0	0	0	0	0	0	0	0	0	0	0	0	0	0	0	0	0	0	0	0	0.42	0	0
RO	0	0	0.34	0	0	0	0	0	0	0	0	0.45	0	0	0	0	0	0	0	0	0	0	0	0	0	0
SK	0.42	0	0	0	0.32	0	0	0	0	0	0	0.17	0	0	0	0	0	0	0.38	0	0	0	0	0	0	0
SI	0.17	0	0	0.17	0	0	0	0	0	0	0	0.37	0	0.43	0	0	0	0	0	0	0	0	0	0	0	0
ES	0	0	0	0	0	0	0	0	0.87	0	0	0	0	0	0	0	0	0	0	0.42	0	0	0	0	0	0
SE	0	0	0	0	0	0.8	0	0.53	0	1.31	0	0	0	0	0	0.9	0	0.48	1.16	0	0	0	0	0	0	0
CH	0.46	0	0	0	0	0	0	0	0.44	0.5	0	0	0	0.55	0	0	0	0	0	0	0	0	0	0	0	0

Authorized licensed use limited to: TU Delft Library. Downloaded on April 21,2026 at 11:19:51 UTC from IEEE Xplore. Restrictions apply.

TABLE III: Parameters used in the EEA-ENB.

τ	$\tau_{\mathrm{T},i}$	$\tau_{\mathrm{R},i}$	$K_{\mathrm{p},i}$	T_{ij}
0.25 [s]	2.5 [s]	25 [s]	0.05 $\left[\frac{\mathrm{Hz}}{\mathrm{GW}}\right]$	$\frac{1}{d_{ij}}$ $\left[\frac{\mathrm{GW}}{\mathrm{deg}}\right]$

IV. THE EEA-HENB MODEL

A. System Description

The model of each electrical area $\mathcal{A}_i \in \mathcal{V}$ of the EEA electricity network is composed by the connection of an equivalent electrical machine and an ESS, as reported in the schematic in Fig. 2. An equivalent machine is generally made of a turbine and a rotary mass [24, 31]. The turbine converts energy (e.g. mechanical) into electricity, and the actual process depends by the power generation technology. The rotary mass is the mass of the rotor of the turbine, which in traditional turbines contains the magnets responsible for the electricity production through current induction on the stator [32]. In our model, we make the following assumptions about the equivalent electrical machines:

- Each machine aggregates the power generation capabilities and inertia of all dispatchable energy resources in an area[1].
- We work at a time scale (i.e. $\tau = 2.5$ [s]) such that every energy request at the control time instants of the turbine is satisfied instantaneously [24]. This approach focuses on the secondary level control loop of an electrical machine [25]. Accordingly, we neglect dynamics at a time scale below the sampling time $\tau = 2.5$ [s], such as turbine dynamics, while retaining the behavior of the rotating mass.
- The model for the rotating mass of the i-th equivalent electrical machine is a first-order low pass filter with time constant $\tau_{\mathrm{R},i} = 25$ [s], $\forall i$.

Regarding the ESS, we assume a Piecewise-Affine Linear (PWA) dynamics, which depends on its input-state configuration, thus being a hybrid system. This approach is similar to the one that can be found in [26, 27]. However, we extend it by adding different charging and discharging rates, as explained in next section.

B. The mathematical model

From the modeling assumptions above and the available data, we obtain a model of the equivalent electrical areas that, for each area i, is constituted by:

- Two control inputs, which are the variation in the dispatchable energy allocation of the turbine of the i-th electrical machine $\Delta P_i^{\mathrm{disp}}$; and the energy P_i^{ESS} exchanged with the ESS.
- Two external and known inputs, which are the load request variation $\Delta P_i^{\mathrm{load}}$, and the variation in renewable energy generation production $\Delta P_i^{\mathrm{ren}}$. These signals are generated according to [19].
- A dynamical coupling signal representing the power exchange between the i-th area and its electrical neighbors $j \in \mathcal{N}_i$, i.e. $\Delta P_i^{\mathrm{tie}}$. This signal, which is an incremental quantity, is obtained considering the deviation between the electrical angles of each couple of equivalent electrical areas. This angle is one of the states of the respective systems, and is introduced in the next points.
- Five states, which are: i) the variation of the frequency of the equivalent machine Δf_i w.r.t. the nominal operating frequency $f_0 = 50$ [Hz]; ii) the variation of the machine angle $\Delta\delta_i$ [deg] w.r.t. the nominal angle δ_0; iii) the energy e_i [GWh] stored inside the ESS; iv) the dispatchable power allocation P_i^{disp} of the i-th area that is obtained as the series sum of the initial allocation at time step 0 and of the variations in dispatchable power allocation $\Delta P_i^{\mathrm{disp}}$; v) the total energy exchange over the tie-lines P_i^{tie} of the i-th area, obtained as the series sum of the increments $\Delta P_i^{\mathrm{tie}}$ of the power transmitted over the tie-lines.

TABLE IV: Values of the energy rate η_i^j for the ESS i, depending on the input-state configuration Ω^j, for $j = 1, \ldots, 8$.

Energy level [%]	$P_i^{\mathrm{ESS}}(k) \geq 0$	$P_i^{\mathrm{ESS}}(k) < 0$
$0 \leq e_i(k) < 25$	$\eta_i^1 = 0.9$	$\eta_i^5 = \frac{1}{0.9}$
$25 \leq e_i(k) < 50$	$\eta_i^2 = 0.8$	$\eta_i^6 = \frac{1}{0.8}$
$50 \leq e_i(k) < 75$	$\eta_i^3 = 0.7$	$\eta_i^7 = \frac{1}{0.7}$
$75 \leq e_i(k) \leq 100$	$\eta_i^4 = 0.6$	$\eta_i^8 = \frac{1}{0.6}$

The resulting dynamics associated with the i-th area $\mathcal{A}_i$ is provided by the system of PWA equations:

$$\begin{aligned}
&\Delta\delta_i(k+1) = \Delta\delta_i(k) + \tau 2\pi \Delta f_i(k) \\
&\Delta f_i(k+1) = \left(1 - \tfrac{\tau}{\tau_{\mathrm{R},i}}\right) \Delta f_i(k) + K_{\mathrm{p},i} \tfrac{\tau}{\tau_{\mathrm{R},i}} g_i(k) \\
&e_i(k+1) = e_i(k) + \tau \eta_i^j P_i^{\mathrm{ESS}}(k) \text{ for } \begin{bmatrix} e_i(k) \\ P_i^{\mathrm{ESS}}(k) \end{bmatrix} \in \Omega^j \quad (1) \\
&P_i^{\mathrm{disp}}(k+1) = P_i^{\mathrm{disp}}(k) + \tau \Delta P_i^{\mathrm{disp}}(k) \\
&P_i^{\mathrm{tie}}(k+1) = P_i^{\mathrm{tie}}(k) + \tau \Delta P_i^{\mathrm{tie}}(k)
\end{aligned}$$

with:

$$\begin{aligned}
g_i(k) = \Delta P_i^{\mathrm{disp}}(k) - \Delta P_i^{\mathrm{load}}(k) + \Delta P_i^{\mathrm{ren}}(k) + \\
- \Delta P_i^{\mathrm{tie}}(k) - P_i^{\mathrm{ESS}}(k) \quad (2)
\end{aligned}$$

$$\Delta P_i^{\mathrm{tie}}(k) = \sum_{j \in \mathcal{N}_i} T_{ij} (\Delta\delta_i(k) - \Delta\delta_j(k)) \quad (3)$$

and $T_{\mathrm{p},i}$, $K_{\mathrm{p},i}$, are respectively the gain and the time constant of the dynamics of the rotating mass; and T_{ij} is the gain associated with the tie-line connecting nodes i and j. The gain T_{ij} associated with the tie-line is related to the geographical distance d_{ij} reported in Table II by the relation $T_{ij} = \frac{k_{ij}}{d_{ij}}$, where $k_{ij} = 1$ is a tuning parameter, assumed unitary in this description, but more refined characterization might consider the impedance per kilometer of the tie-line. All parameters are reported in Table III.

[1] A relaxation of this type of assumption was performed in [26], where multiple generators are activated according to binary decision variables. Such approach can be useful if a deregulated energy market model has to be implemented, as described in [25].

Authorized licensed use limited to: TU Delft Library. Downloaded on April 21,2026 at 11:19:51 UTC from IEEE Xplore. Restrictions apply.

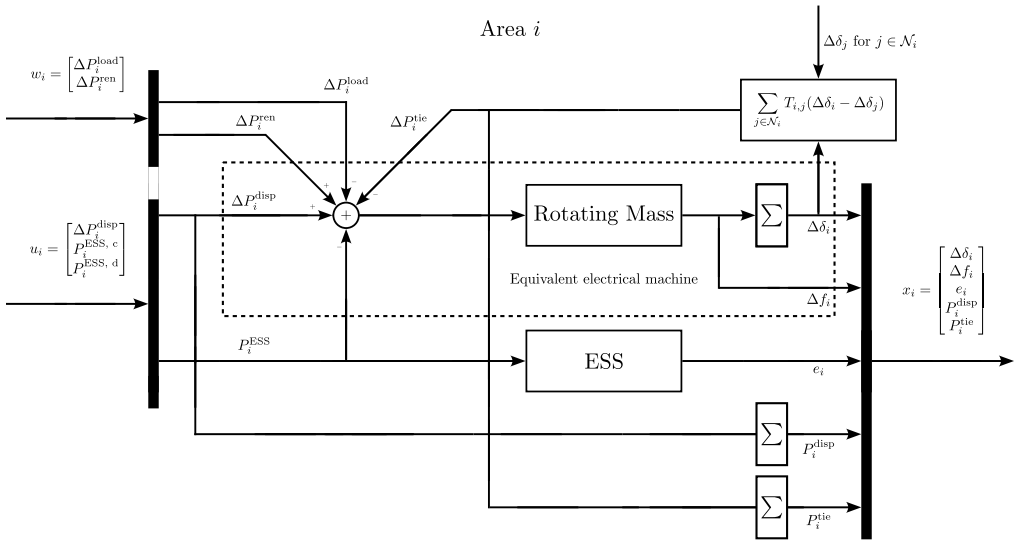

Fig. 2: Schematic of the i-th electrical area.

C. The Mixed Logical Dynamical Formulation

Regarding the PWA formulation of the ESS dynamics, the parameter η_i^j incorporates the charging or discharging rates of the ESS on the basis of the input-state configuration j. In general, this is done by selecting a value of the parameter η_i^j as:

$$\eta_i^j \text{ for } \underline{e}_i^j \leq e_i(k) < \overline{e}_i^j \ \wedge \ \left[P_i^{\text{ESS}}(k) \geq 0 \vee P_i^{\text{ESS}}(k) < 0\right], \tag{4}$$

where $\underline{e}_i^j$ and $\overline{e}_i^j$ are respectively the lower and upper bounds of the energy level in which the rate η_i^j is valid, and $P_i^{\text{ESS}}(k)$ defines the configuration of the input. The rates that we propose are reported in Table IV, where our choice is purely illustrative. However, these parameters can be selected to accurately represent specific ESSs technologies.

The dynamics reported in (1)-(3) can be reformulated into a Mixed Logical Dynamical (MLD) form, as described in [10]. To this end, we introduce the binary variables φ^{ESS}, and auxiliary variables z^{ESS}, to convert the ESSs dynamics from PWA into MLD representation. Specifically, for each area i, we introduce as many φ_i^{ESS} and z_i^{ESS} as are the operating modes of the ESSs reported in Table IV. We define φ_i^{ESS} such that $\varphi_i^{\text{ESS},j}(k) = 1$ if and only if the system is in the operating mode j at time step k. Then, we rewrite the ESS dynamics as:

$$e_i(k+1) = e_i(k) + \tau \sum_{j=1}^{8} \eta_i^j \varphi_i^{\text{ESS},j}(k) P_i^{\text{ESS}}(k), \tag{5}$$

and the nonlinearity is removed using the auxiliary variables $z_i^{\text{ESS},j} = \eta_i^j \varphi_i^{\text{ESS},j}(k) P_i^{\text{ESS}}(k)$, thus obtaining:

$$e_i(k+1) = e_i(k) + \tau \sum_{j=1}^{8} z_i^{\text{ESS},j}(k). \tag{6}$$

Equation (6) is subject to the set of linear inequality constraints defined according to [10, 26]:

$$E_{i,2}^{\text{ESS}} \varphi_i^{\text{ESS}}(k) + E_{i,3}^{\text{ESS}} z_i^{\text{ESS}}(k) \leq E_{i,1}^{\text{ESS}} u_i(k) + E_{i,5}^{\text{ESS}} \tag{7}$$

where φ_i^{ESS} and z_i^{ESS} are the vectors containing respectively $\varphi_i^{\text{ESS},j}$ and $z_i^{\text{ESS},j}$ for $j = 1, \ldots, 8$.

Finally, we can rewrite the aggregated dynamics of the EEA-HENB. To this, we denote the state, the input, the auxiliary variables, and the external signal vectors of the i-th area respectively by:

$$\begin{aligned} &x_i^\intercal = [\Delta\delta_i \ \Delta f_i \ e_i \ P_i^{\text{disp}} \ P_i^{\text{tie}}]^\intercal \quad u_i^\intercal = [\Delta P_i^{\text{disp}} \ P_i^{\text{ESS}}]^\intercal \\ &z_i^\intercal = [z_i^{\text{ESS},1} \ \cdots \ z_i^{\text{ESS},8}]^\intercal \quad \varphi_i^\intercal = [\varphi_i^{\text{ESS},1} \ \cdots \ \varphi_i^{\text{ESS},8}]^\intercal \\ &w_i^\intercal = [\Delta P_i^{\text{load}} \ \Delta P_i^{\text{ren}}]^\intercal \end{aligned} \tag{8}$$

Then, for the overall system with $N = 26$ areas, we aggregate these vectors into global vectors as $x^\intercal = [x_1^\intercal \ \cdots \ x_{26}^\intercal]^\intercal$, $u^\intercal = [u_1^\intercal \ \cdots \ u_{26}^\intercal]^\intercal$, $z^\intercal = [z_1^\intercal \ \cdots \ z_{26}^\intercal]^\intercal$, $\varphi^\intercal = [\varphi_1^\intercal \ \cdots \ \varphi_{26}^\intercal]^\intercal$, and $w^\intercal = [w_1^\intercal \ \cdots \ w_{26}^\intercal]^\intercal$. In conclusion, the system dynamics with the respective constraints are:

$$x(k+1) = Ax(k) + B^{\text{u}}u(k) + +B^{\text{z}}z(k) + Dw(k) \tag{9}$$

$$E_2\varphi(k) + E_3 z(k) \leq E_1 u(k) + E_4 x(k) + E_5 \tag{10}$$

V. Benchmark Empirical Validation

To asses the potential of the benchmark as a tool to test multi-agent distributed control strategies, we propose two settings, representing test cases that can be implemented directly, or adapted according to the research requirement. For the sake of simplicity, we use only two sub-parts of the network, but test cases for the entire benchmark network can be easily implemented, at the expense of longer computation time and increased complexity. For example, in [19] we tested the entire network using linear dynamics for CMPC over a day of operation, and for that case the computation required several days of execution. First, we perform the control simulation of part of the network using a centralized MPC approach. Then, we implement a distributed MPC control scheme using the Alternating Direction Method of Multipliers (ADMM) [33]. We performed the simulations with a CPU Intel core i7-1185G7.

Authorized licensed use limited to: TU Delft Library. Downloaded on April 21,2026 at 11:19:51 UTC from IEEE Xplore. Restrictions apply.

A. Centralized MPC

For this setting, we consider the subnetwork constituted by the electrical areas $\mathcal{V} = \{2, 5, 8, 9, 10, 13, 14, 17, 18, 19, 24, 25, 26\}$, which are selected arbitrarily. We implement a centralized MPC strategy using the same settings as in [19], the set of parameters used can be accessed through the software repository [18], and their choice is made by expert selection for grid stability. In particular, we want to limit the deviation of the operating frequency and of the machine angles deviations as much as possible, ensuring the satisfaction of operational bounds: $|\Delta\delta_i| \leq 3.5$, $|\Delta f_i| \leq 0.05$, for all i. Additionally, we want to accumulate energy in the ESSs, bringing them from an initial value of $3 \cdot e_i^{\max}/7$ to $4 \cdot e_i^{\max}/7$, with $e_i^{\max}$ being the maximum storage capacity of area i. These values are arbitrary and used with the only purpose that the energy storage system switches between at least two operational modes. The resulting simulation is reported in Figure 3. Performing this simulation consisting of 300 steps required 3137 [s]. Also, in the MPC implementation, we used measurements of the external signals for the current time step, and forecasts for the others, which allows to empirically asses the robustness of the formulation w.r.t. signal variation. This discrepancy in the knowledge of external signals introduces some oscillations in the controlled dynamics. Moreover, from the simulation we can appreciate that it is possible to set reference values for the level of charge of the ESS, at the expenses of some further increase of oscillatory behaviors in the frequency and machine angle. A similar approach can be used to minimize the total level of dispatchable energy used for control, which can result in consistent economical gains in network operations. We conclude that the centralized MPC strategy ensures the operation of the network under constraints and using forecasts of data. The results of the centralized control approach can be used to validate and compare non-centralized control strategy from the perspective of optimality, computation time and resources.

B. ADMM-based Distributed MPC

We implement an alternating direction method of multipliers (ADMM)-based distributed MPC strategy [34] to show a possible application of the benchmark in the study of multi agents systems. For this simulation we consider the set of areas $\mathcal{V} = \{9, 10, 13, 14, 17, 26\}$. In this setting, we require to minimize deviation of the sate values from references, as above. However, we do not set any reference for the ESSs behavior. In this setting, each electrical area is considered as an independent control agent. The resulting behavior for the machine angle and frequency deviations are reported in Figure 4.

VI. CONCLUSIONS AND FUTURE WORK

In this article, we presented the hybrid formulation of a benchmark for the control of an electrical network representing an abstraction of the European economic area electricity network. The benchmark is suited for implementing and comparing control strategies for a network of dynamical systems with a certain level of scale and complexity. The benchmark is characterized by official topological and electrical data. All processed data and source codes are provided in a long-term repository access for future studies. We demonstrated the capabilities of the benchmark by first testing a centralized MPC strategy, with desired energy storage behavior, and then ADMM-based distributed MPC strategies. We found that this system exhibits peculiar features that can be relevant in testing and comparing centralized and distributed control approaches in the framework of hybrid network systems.

Future work can be directed towards enhancing the complexity and the features of the benchmark, such as considering the implementation of deregulated energy market setting, primary frequency control loops, economic optimization including energy prices, uncertainties on energy forecasts in a stochastic framework, and advanced logic-driven features such as plug-and-play operations and vehicle-to-grid systems. Moreover, further studies regarding different MPC formulations can be devised, including comparisons of performance and scalability with different centralized and distributed strategies, design and validation of robust formulations, and assessment of performance and stability w.r.t. MPC parameters variation. Finally, the evaluation of the control performance of the architecture can benefit from the introduction of more advanced metrics as computational efficiency, energy cost minimization, or grid reliability.

REFERENCES

[1] D. D. Šiljak. *Large-Scale Dynamic Systems: Stability and Structure*. Dover Publications Inc., 2008. 416 pp.

[2] M. Kordestani, A. A. Safavi, and M. Saif. "Recent survey of large-scale systems: Architectures, controller strategies, and industrial applications". In: *IEEE Systems Journal* 15 (2021), pp. 5440–5453.

[3] G. Weiss, ed. *Multiagent Systems*. Second Edition. MIT Press, 2013. 867 pp.

[4] D. D. Šiljak. *Decentralized Control of Complex Systems*. Academic Press, Inc., 1991.

[5] R. Scattolini. "Architectures for distributed and hierarchical model predictive control – A review". In: *Journal of Process Control* 19 (2009), pp. 723–731.

[6] F. Fele, J. M. Maestre, and E. F. Camacho. "Coalitional control: Cooperative game theory and control". In: *IEEE Control Systems Magazine* 37 (2017), pp. 53–69.

[7] L. Busoniu, R. Babuska, and B. De Schutter. "A comprehensive survey of multiagent reinforcement learning". In: *IEEE Transactions on Systems, Man, and Cybernetics, Part C (Applications and Reviews)* 38 (2008), pp. 156–172.

[8] P. Tabuada. *Verification and Control of Hybrid Systems: A Symbolic Approach*. Springer, 2009.

[9] E. Sontag. "Nonlinear regulation: The piecewise linear approach". In: *IEEE Transactions on Automatic Control* 26 (1981), pp. 346–358.

[10] A. Bemporad and M. Morari. "Control of systems integrating logic, dynamics, and constraints". In: *Automatica* 35 (1999), pp. 407–427.

[11] W. P. M. H. Heemels, B. De Schutter, and A. Bemporad. "Equivalence of hybrid dynamical models". In: *Automatica* 37 (2001), pp. 1085–1091.

[12] C. Ju, P. Wang, L. Goel, and Y. Xu. "A two-layer energy management system for microgrids with hybrid energy storage considering degradation costs". In: *IEEE Transactions on Smart Grid* 9 (2018), pp. 6047–6057.

Authorized licensed use limited to: TU Delft Library. Downloaded on April 21,2026 at 11:19:51 UTC from IEEE Xplore. Restrictions apply.

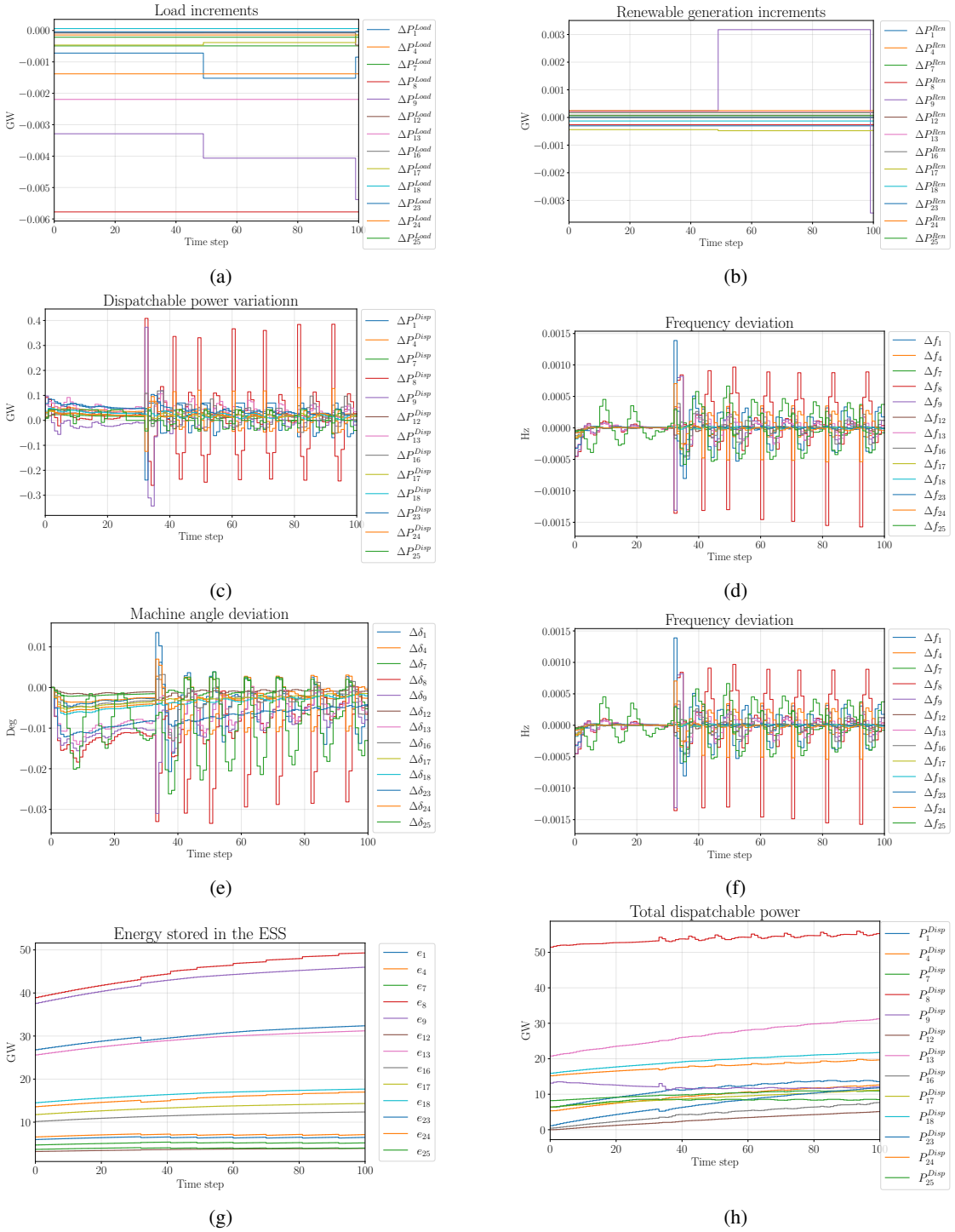

Fig. 3: Simulation using centralized MPC control, with requirements on the desired amount of energy to store in the ESSs.

[13] D. P. e Silva, J. L. Félix Salles, J. F. Fardin, and M. M. Rocha Pereira. "Management of an island and grid-connected microgrid using hybrid economic model predictive control with weather data". In: *Applied Energy* 278 (2021), p. 20.

[14] A. J. del Real, A. Arce, and C. Bordons. "Hybrid model predictive control of a two-generator power plant integrating photovoltaic panels and a fuel cell". In: *2007 46th IEEE Conference on Decision and Control*. 2007, pp. 5447–5452.

[15] M. Hajiahmadi, J. Haddad, B. De Schutter, and N. Geroliminis. "Optimal hybrid perimeter and switching plans control for urban traffic networks". In: *IEEE Transactions on Control Systems Technology* 23 (2015), pp. 464–478.

[16] A. Núñez, C. Ocampo-Martinez, J. M. Maestre, and B. De Schutter. "Time-varying scheme for noncentralized model predictive control of large-scale systems". In: *Mathematical Problems in Engineering* 2015 (2015), pp. 1–17.

[17] F. Alavi, E. Park Lee, N. van de Wouw, B. De Schutter, and Z. Lukszo. "Fuel cell cars in a microgrid for synergies between hydrogen and electricity networks". In: *Applied Energy* 192 (2017), pp. 296–304.

Authorized licensed use limited to: TU Delft Library. Downloaded on April 21,2026 at 11:19:51 UTC from IEEE Xplore. Restrictions apply.

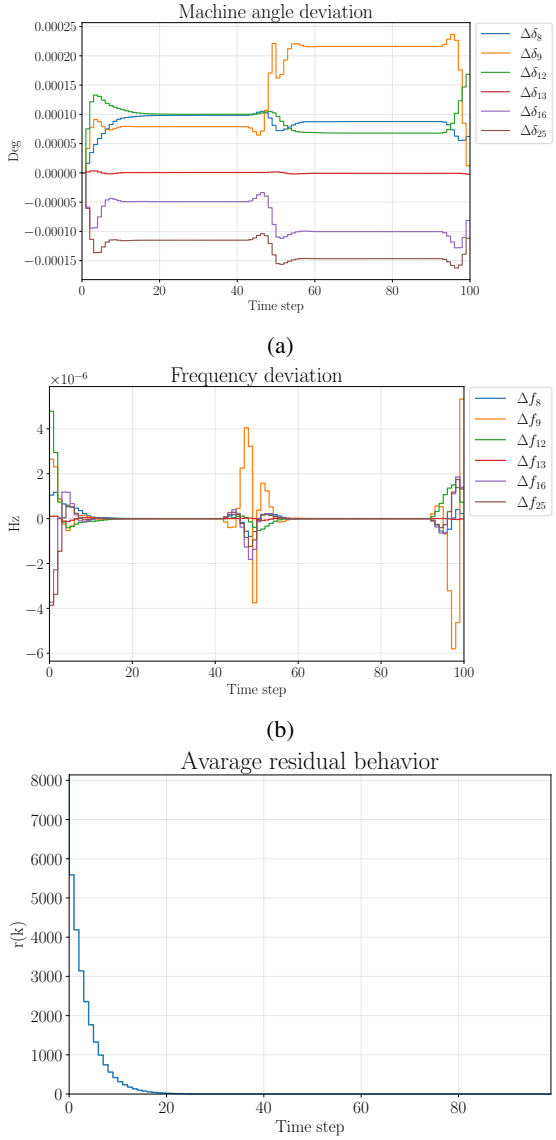

Fig. 4: Behavior of the states and of the residual for the DMPC-ADMM strategy.

[18] A. Riccardi, L. Laurenti, and B. De Schutter. *Code underlying the publication: A benchmark for multi-agent control of energy systems: The European economic area hybrid electricity network benchmark*. 2024. URL: https://doi.org/10.4121/185ef121-22b7-4679-90ba-f57e1b40c5db.

[19] A. Riccardi, L. Laurenti, and B. De Schutter. "A benchmark for the application of distributed control techniques to the electricity network of the European economic area". In: *Control Systems Benchmarks*. Springer, 2025. URL: http://arxiv.org/abs/2403.14372.

[20] A. Riccardi, L. Laurenti, and B. De Schutter. *Code underlying the publication: A benchmark for the application of distributed control techniques to the electricity network of the European economic area*. 2024. URL: https://doi.org/10.4121/d2c0d075-1c49-41af-8113-5e50c27ca97e.

[21] A. Riccardi, L. Laurenti, and B. De Schutter. "A generalized partitioning strategy for distributed control". In: *2024 63nd IEEE Conference on Decision and Control (CDC)*. 2024, *accepted*, p. 8.

[22] A. Riccardi, L. Laurenti, and B. De Schutter. *Code underlying the publication: A generalized partitioning strategy for distributed control*. 2024. URL: https://doi.org/10.4121/90ada13d-a6c9-4e4c-a046-2b984595bcdd.

[23] M. Ranjan and R. Shankar. "A literature survey on load frequency control considering renewable energy integration in power system: Recent trends and future prospects". In: *Journal of Energy Storage* 45 (2022), p. 33.

[24] P. Kundur. *Power System Stability and Control*. McGraw-Hill, 1993. 199 pp.

[25] H. Bevrani. *Robust Power System Frequency Control*. Springer, 2014. 401 pp.

[26] T. Pippia, J. Sijs, and B. De Schutter. "A single-level rule-based model predictive control approach for energy management of grid-connected microgrids". In: *IEEE Transactions on Control Systems Technology* 28 (2020), pp. 2364–2376.

[27] A. Parisio, E. Rikos, and L. Glielmo. "A model predictive control approach to microgrid operation optimization". In: *IEEE Transactions on Control Systems Technology* 22 (2014), pp. 1813–1827.

[28] *NUTS*. GISCO - Eurostat. URL: https://ec.europa.eu/eurostat.

[29] *Grid Map*. Entso-E. URL: https://www.entsoe.eu/data/map/.

[30] *ENTSO-E transparency platform*. The European network of transmission system operators. URL: https://transparency.entsoe.eu/.

[31] C. E. Fosha and O. I. Elgerd. "The megawatt-frequency control problem: A new approach via optimal control theory". In: *IEEE Transactions on Power Apparatus and Systems* 89 (1970), pp. 563–577.

[32] P. Krause, O. Wasynczuk, S. Sudhoff, and S. Pekarek. *Analysis of Electric Machinery and Drive Systems*. Third edition. Wiley-IEEE Press, 2013. 680 pp.

[33] S. Boyd, N. Parikh, E. Chu, B. Peleato, and J. Eckstein. "Distributed optimization and statistical learning via the alternating direction method of multipliers". In: *Foundations and Trends in Machine Learning* 3 (2010), p. 122.

[34] T. H. Summers and J. Lygeros. "Distributed model predictive consensus via the alternating direction method of multipliers". In: *50th Annual Allerton Conference on Communication, Control, and Computing*. 2012, pp. 79–84.

Authorized licensed use limited to: TU Delft Library. Downloaded on April 21,2026 at 11:19:51 UTC from IEEE Xplore. Restrictions apply.